JOURNAL OF MATERIALS SCIENCE 28 (1993) 3347–3352

Visco-elasticity in alumina ceramics at room temperature

A. T. YOKOBORI JR, C. Y. JIAN
Faculty of Engineering, Tohoku University, Sendai, Japan
T. ADACHI
Faculty of Science and Engineering, Ishinomaki Senshu University, Ishinomaki, Miyagi, Japan
T. YOKOBORI
School of Science and Engineering, Teikyo University, Utsunomiya, Tochigi, Japan

The decrease in the fracture strength of alumina ceramics at room temperature has usually been assumed to be caused by the effect of stress corrosion. However, at high temperatures, a viscous deformation will occur due to a glass-like phase which exists in the grain boundary. A study of the relation of the fracture strength of an alumina ceramics smooth specimen at room temperature to the visco-elastic property was performed. Mechanical tests and visco-elastic analysis, has shown that the fracture strength of this kind is controlled by the visco-elasticity.

1. Introduction

The decrease in the fracture strength of alumina ceramics at room temperature has generally been assumed to be caused by the effect of stress corrosion [1, 2]. On the other hand, a viscous deformation will occur at high temperatures due to a glass-like phase which exists in the grain boundary.

The relationship between the fracture strength of an alumina ceramics smooth specimen at room temperature and its visco-elastic property, has been studied. Using mechanical tests and visco-elastic analysis, it has been shown that the fracture strength of this kind is controlled by the visco-elasticity.

2. Materials and specimens

The specimens used were 96% and 92% purity alumina ceramics with the chemical composition shown in Table I. Specimen dimensions were 60 mm (length) × 10 mm (width) × 1 mm (thickness) for 96% alumina ceramics and 70 mm (length) × 4 mm (width) × 1.5 mm (thickness) for 92% alumina ceramics.

3. Dynamic fatigue test and interpretation

A dynamic fatigue test was carried out using the four-point bending method at different crosshead speeds (0.03–25 mm min^{-1}) at room temperature in air and water, respectively. The major span of the specimen was 30 mm and the minor span was 10 mm.

In Fig. 1a and b the fracture strength is plotted against the logarithm of stress rate for 96% and 92% alumina ceramics, respectively. The results are shown in Fig. 2 as obtained by the least square method. Fig. 2 shows that fracture strength increases almost linearly with the logarithm of stress rate [3, 4]. It should be noted that the fracture strength is lower in water than in air and that the gradient of the straight line is much smaller in water than in air for each material of different purity.

To determine the mechanism of this behaviour, first let us consider whether or not the controlling mechanism may be a reaction rate process, such as corrosion cracking as is usually assumed. If the rate-controlling mechanism is the reaction rate process, whatever the detailed mechanism may be, the rate of atomic rearrangement, m, can be written in the simple form

$$m = A \exp\left(-\frac{H - \alpha\sigma}{kT}\right) \quad (1)$$

where H is the activation energy, α the activated volume, σ the applied stress, T the absolute temperature, k Boltzmann's constant and A the frequency factor. By treating the process as a stochastic one, then we can obtain the fracture strength, σ_c, from the following equation [5]

$$\frac{dm}{dt} = m^2 \quad (2)$$

TABLE I Chemical composition for an average grain diameter of 2.33 μm

Al_2O_3	96%	92%
SiO_2	4%	7%
CaO		1%
MgO		–
Grain diameter	4.33 μm	2.33 μm

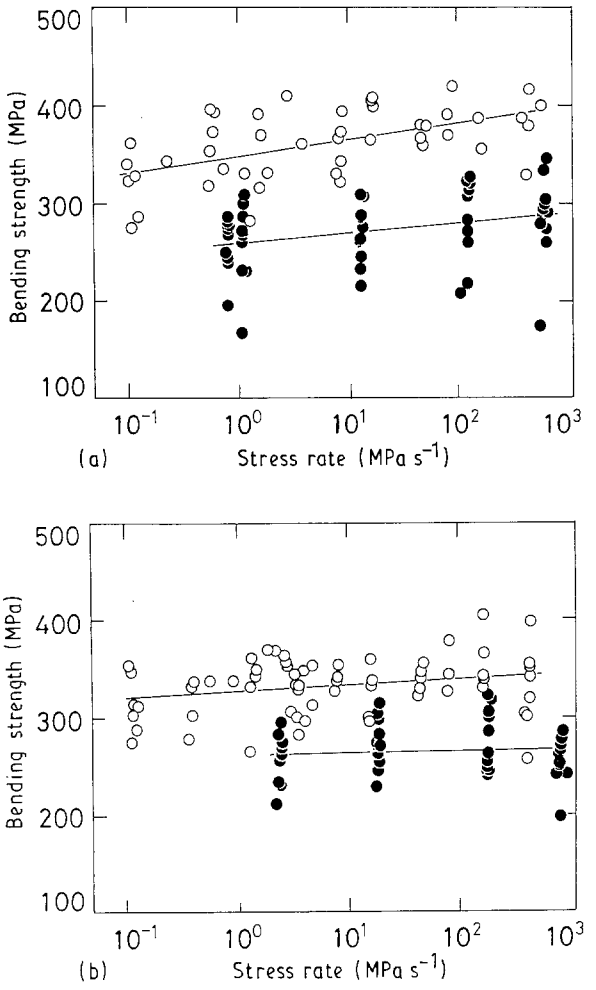

Figure 1 Experimental data on dynamic fatigue strength of alumina ceramics versus the logarithm of stress rate in (a) air, and (b) water. (○) 96% alumina, (●) 92% alumina.

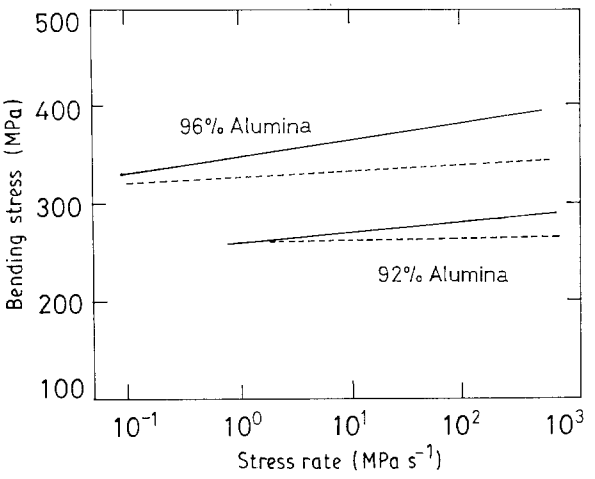

Figure 2 The relationship of dynamic fatigue strength versus the logarithm of stress rate of alumina ceramics (96% and 92% purity) in (——) air and (– – –) water determined by the least squares method from the data in Fig. 1a and b.

for the case of constant rate of stress application, i.e. $\sigma = \dot{\sigma}t$, where $\dot{\sigma}$ is the applied stress rate. From Equations 1 and 2, we obtain the fracture strength, σ_c, as

$$\sigma_c = \frac{kT}{\alpha}\left(\log\dot{\sigma} + \frac{H}{kT} + \log\frac{1}{A} + \log\frac{\alpha}{kT}\right) \quad (3)$$

Experimentally, for the case of glass, the gradient of the curve of fracture strength, σ_c, against $\log\dot{\sigma}$ is much smaller in air than in water, the fracture strength itself in air being higher than in water. This gradient characteristic may be explained by assuming the activation volume α, is much larger in air than in water, as can be seen from Equation 3. On the other hand, from the present experimental data as shown in Fig. 2, the gradient of the curve in water is much smaller than in air. Therefore, the rate-controlling mechanism for fracture of this type might not be a reaction rate process mechanism, such as corrosion cracking. Thus an attempt has been made to analyse the behaviour based on a visco-elastic model.

4. Analysis based on a visco-elastic model

Simulation analysis was performed by using a visco-elastic spring model shown in Fig. 3a. The basic equations of this model are expressed by

$$\sigma = E_3\varepsilon_3 = E_1(\varepsilon_2 + \varepsilon_\eta) + E_2\varepsilon_2 \quad (4)$$

$$E_2\varepsilon_2 = \eta\frac{d\varepsilon_\eta}{d\eta} \quad (5)$$

and total strain is

$$\varepsilon = \varepsilon_2 + \varepsilon_3 + \varepsilon_\eta \quad (6)$$

Substituting Equations 4 and 5 into Equation 6, we have

$$\varepsilon_\eta = \frac{AB}{\eta}\exp\left(-\frac{AC}{\eta}t\right)\int_0^t \varepsilon\exp\left(\frac{AC}{\eta}t\right)dt + C_0\exp\left(-\frac{AC}{\eta}t\right) \quad (7)$$

where $A = 1/(E_1 + E_2 + E_3)$, $B = E_2 \times E_3$, $C = E_2(E_1 + E_3)$, and C_0 is an arbitrary constant.

The strain rate, V, in the dynamic fatigue test is expressed by the following equation

$$\varepsilon = Vt \quad (8)$$

The initial condition is

$$\varepsilon_\eta = 0 \quad \text{for } t = 0. \quad (9)$$

Substituting Equations 8 and 9 into Equation 7, ε_η is expressed as

$$\varepsilon_\eta = \frac{BV}{C}\left(t - \frac{\eta}{AC}\right) + \frac{B\eta V}{AC^2}\exp\left(-\frac{AC}{\eta}t\right) \quad (10)$$

Therefore, from Equation 10, the stress, σ, is obtained as follows

$$\sigma = E_3\left\{Vt - \frac{BV}{C}t + \frac{BV\eta}{C}\left[\frac{1}{AC} - \frac{1}{E_2} - \left(1 - \frac{AC}{E_2}\right)\frac{1}{AC}\exp\left(-\frac{AC}{\eta}t\right)\right]\right\} \quad (11)$$

Fig. 3b shows the calculated result from Equation 11 assuming the critical strain criterion,

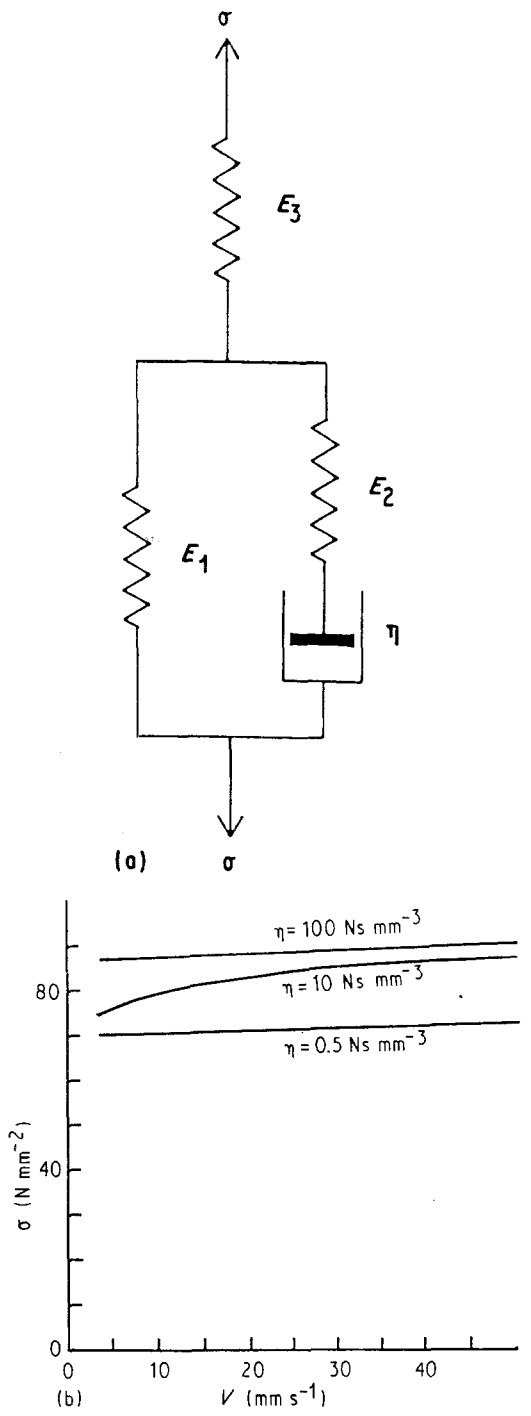

Figure 3 (a) The visco-elastic model. (E_1, E_2, E_3 are values of Young's modulus, η is the viscosity.) (b) Characteristics of dynamic fatigue strength versus strain rate calculated by simulation based on the visco-elastic model as shown in (a). $E_1 = 10\,\mathrm{N\,mm^{-2}}$, $E_2 = 20\,\mathrm{N\,mm^{-2}}$, $E_3 = 5\,\mathrm{N\,mm^{-2}}$.

where $E_1 = 10\,\mathrm{N\,mm^{-2}}$, $E_2 = 20\,\mathrm{N\,mm^{-2}}$ and $E_3 = 5\,\mathrm{N\,mm^{-2}}$, and $\eta = 0.5$, 10 and 100 $\mathrm{Ns\,mm^{-2}}$, respectively. Fig. 3b shows that for a high coefficient of viscosity ($\eta = 100\,\mathrm{Ns\,mm^{-2}}$) the visco-elastic spring model is approximately equal to the model consisting of elastic springs E_1, E_2 and E_3, and fracture strength is almost constant and independent of strain rate. On the other hand, when η decreases greatly ($\eta = 0.5\,\mathrm{Ns\,mm^{-2}}$), the visco-elastic spring model behaves as a spring model which consists of E_1 and E_3 connected in series. In this case, fracture strength becomes lower, but it is also independent of strain rate. When viscosity assumes an intermediate value ($\eta = 10\,\mathrm{Ns\,mm^{-2}}$), the fracture strength increases with increase in strain rate. This behaviour corresponds to a strain-rate dependence.

From Fig. 3b it has been found that the characteristic dependence of fracture strength, σ_c, on viscosity varies within the range of the value of viscosity. That is, it can be seen that the characteristic of the gradient of fracture strength, σ_c, of alumina ceramics being smaller in water than in air, as shown in Fig. 2b, corresponds to the case when the viscosity is smaller in water than in air, as shown in Fig. 3b, similar to the examples for $\eta = 10$ and $0.5\,\mathrm{Ns\,mm^{-2}}$.

5. Stress relaxation test and results

A four-point bending method, similar to the dynamic fatigue test, was used. Initial strain was applied at the value which causes an equivalent stress of two-thirds the bending strength under 1 $\mathrm{MPa\,s^{-1}}$ stress rate. The time sequence of this test was 5000 s.

The results from the stress relaxation test are shown in Fig. 4 for 96% alumina ceramics in air and in water. The characteristic of stress relaxation is more remarkable, and at the same time the stress relaxation time becomes shorter in water than in air.

By using the Maxwell model, the relaxation elastic modulus, E_r, for this case can be expressed as

$$\frac{E_r}{E} = \frac{E_1}{E}\exp\left(-\frac{t}{\tau_1}\right) + \frac{E_2}{E}\exp\left(-\frac{t}{\tau_2}\right) + \frac{E_3}{E}\exp\left(-\frac{t}{\tau_3}\right) + \ldots \quad (12)$$

where τ_i is relaxation time which is given by, $\tau_i = \eta_i/E_i$, where η_i is viscosity and E_i is Young's modulus. For this case we obtain:
in air

$$\frac{E_r}{E} = 5.98 \times 10^{-3}\exp\left(-\frac{t}{5.0}\right) + 7.17 \times 10^{-3}\exp\left(-\frac{t}{70}\right) + 9.87 \times 10^{-1}\exp\left(-\frac{t}{1 \times 10^6}\right) \quad (13)$$

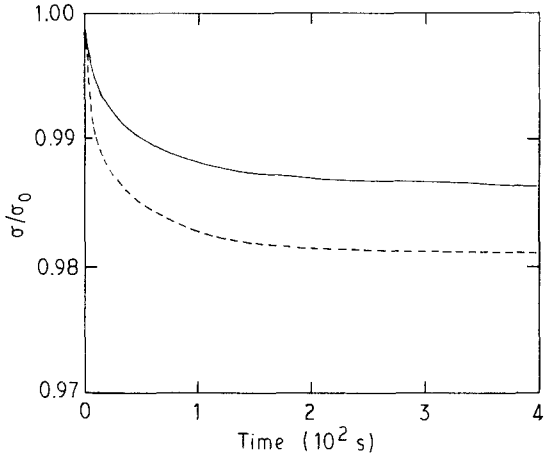

Figure 4 Results of the relaxation test on alumina ceramics (96%) in (——) air and (– – –) water.

in water

$$\frac{E_r}{E} = 9.27 \times 10^{-3} \exp\left(-\frac{t}{3.8}\right) + 9.27 \times 10^{-3} \exp\left(-\frac{t}{50}\right) + 9.81 \times 10^{-1} \exp\left(-\frac{t}{1 \times 10^6}\right) \quad (14)$$

As can be seen from Equations 13 and 14, the second and third terms are much smaller than the first term, and can be neglected. Thus, in air and water the stress relaxation times, τ_{air} and τ_{water}, become, respectively, $\tau_{air} = 5.0$ s and $\tau_{water} = 3.8$ s, where

$$\tau_{air} = \frac{\eta_{air}}{E} \quad (15)$$

and

$$\tau_{water} = \frac{\eta_{water}}{E} \quad (16)$$

6. Internal friction test and results

Fig. 5 shows the resonance apparatus. The experimental apparatus and method are essentially similar as the method of measuring Young's modulus as given in a previous paper [3]. The sine wave generated by an oscillator was amplified to drive a transducer which consists of an electric magnet. In this case, the thin steel plate was adhered to both ends of the specimen, to which the magnetic sinusoidal stress was applied indirectly. The two node points of the specimen were fixed by threads during vibration of both free ends. The value of the internal friction was obtained from half the maximum amplitude in resonance vibration using the following equation

$$\phi = \frac{1}{3^{1/2}} \frac{\nu_2 - \nu_1}{\nu_0} \quad (17)$$

where ν_0 is the resonance frequency and ν_1 and ν_2 are the frequencies at which the amplitude becomes half the maximum, respectively.

From the resonance characteristics, the internal friction, ϕ, was found to be 4.14×10^{-4} in air and 4.42×10^{-4} in humid air. This shows that internal friction is larger in humid air than in air, as shown in Fig. 6. It may be explained as follows: internal friction is expressed by Equation 18 [6].

$$\phi \propto \frac{\omega\tau}{1 + \omega^2\tau^2} \quad (18)$$

where ω is the frequency rate and τ the stress relaxation time. In this experiment, ω is about 600 Hz (Fig. 6) and τ is approximately one order second and, hence, $\omega\tau \gg 1$. In this way, Equation 18 reduces to

$$\phi \propto \frac{1}{\omega\tau} \quad (19)$$

Equations 15, 16 and 19 show that internal friction, ϕ, increases with decreasing τ or viscosity, η. Thus the difference between stress relaxation time in air and in humid air can be understood as caused by the difference between their viscosities.

Furthermore, in Fig. 7 the value of $\tau_{humid\ air}/\tau_{air}$ is plotted against the purity (weight per cent) of alumina, calculated from the data obtained from the internal friction test using Equation 17 and calculated using Equation 19. It can be seen that $\tau_{humid\ air}/\tau_{air}$ or $\eta_{humid\ air}/\eta_{air}$ decreases with increase in amount of added materials, that is, a decrease of Al_2O_3 in the alumina ceramic material from 99.5% to 92%. Probably the glass-phase material added may have contributed to the increase of internal friction or the decrease of viscosity in water.

7. Discussion

The fracture strength of alumina ceramic material increases with increasing stress rate or strain rate [1, 2, 4]. Usually this characteristic has been interpreted as being caused by stress corrosion under water [4, 5]. However, the corrosion reaction is controlled by the

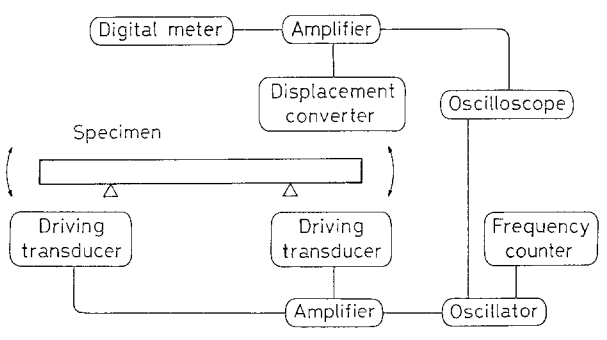

Figure 5 Schematic illustration of the apparatus used for the internal friction test.

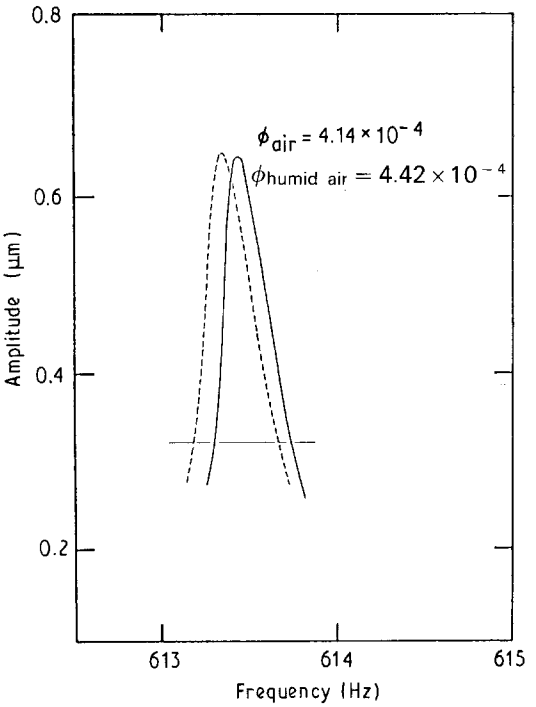

Figure 6 Resonance characteristics of the internal friction test in (——) air and (– – –) humid air.

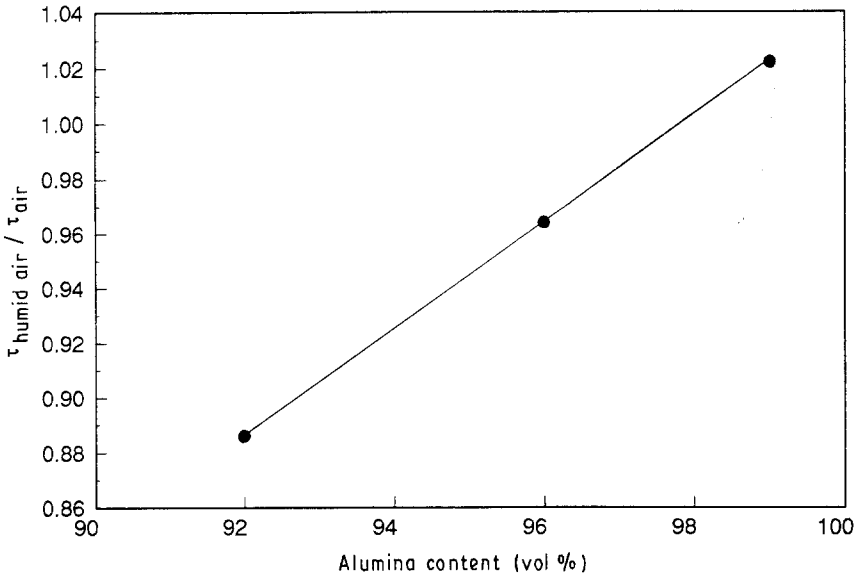

Figure 7 The relation of $\tau_{humid\ air}/\tau_{air}$ to the purity of the alumina ceramics.

reaction rate process mechanism. However, the stress-rate dependence of dynamic fatigue strength of an alumina ceramic smooth specimen at room temperature is smaller in water than in air. On the other hand, if we assume that the rate-controlling process of fracture under these conditions is the reaction rate process, then the gradient of the curve of fracture strength, σ_c, against $\log \dot{\sigma}$ is much smaller in air than in water as shown in Fig. 8. This is not in agreement with the present experimental data as shown in Fig. 2. Instead, a theoretical analysis of behaviour by a visco-elastic model proposed, is in good agreement with the data.

The model may also be supported by the stress relaxation test and the internal friction test. From these experimental results and the theoretical analysis, the alumina ceramic material is supposed to have a visco-elastic property at room temperature. Dynamic fatigue characteristics of the smooth specimen at room temperature can be explained on the basis of a visco-elastic effect which is supposed to come from the glass-like phase in the grain boundary involved in the component added to alumina ceramics, which shows the visco-elastic behaviour.

By controlling the structure, in particular the grain boundary, it may be possible to overcome the brittleness and to improve the ductility and processability at room temperature of a smooth body. This characteristic may be revealed not only in smooth materials, but also in material having short cracks. In the case of a material with long cracks, the corrosion effect may also be involved due to the high stress concentration induced at the crack tip, as shown in Fig. 8. In our experiments, we used thin specimens with, say, large surface area compared with the volume, for dynamic fatigue tests and stress relaxation tests, 60 mm (length) × 10 mm (width) × 1 mm (thickness); for internal friction tests, 120 mm (length) × 10 mm (width) × 1 mm (thickness). This may be the reason why the characteristic is prominent in the present case.

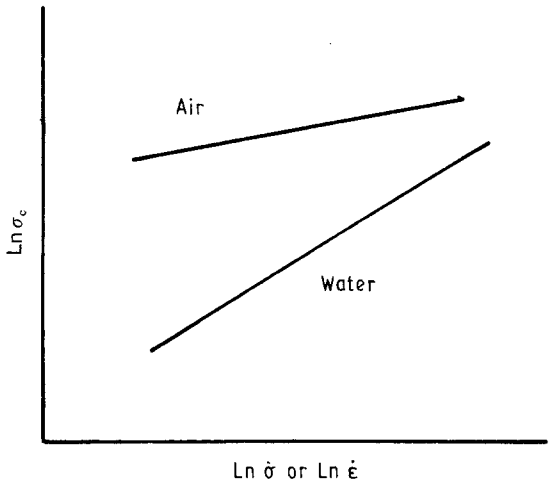

Figure 8 Schematic illustration of dynamic fatigue strength c versus logarithm of stress rate or strain rate for glass materials.

8. Conclusion

Although alumina ceramics are brittle materials, the fracture strength at room temperature was found to be affected by the visco-elastic property of the glass-like phase in the grain boundary. Especially for a smooth specimen, this effect becomes a much more controlling factor, rather than the effect of corrosion. The existence of this property will make it possible to improve the processability by controlling the glass-like phase in the grain boundary.

Acknowledgements

Thanks are extended for the financial aid of this work by research grants from the Ministry of Education, Science and Culture as the Project of Scientific Research on Priority Areas "Advanced Inorganic Materials Mechanical Properties" of which Professor Takeo Yokobori is the Chairman.

References

1. S. M. WIEDERHORN, E. R. FULLER Jr and R. THOMSON, *Metal Sci.* **14** (1980) 450.
2. A. G. EVANS and E. R. FULLER, *Met. Trans.* **5** (1974) 27.
3. A. T. YOKOBORI Jr, T. ADACHI, T. YOKOBORI, H. ABE, J. NAKAYAMA, H. TAKAHASHI and H. MIYATA, in "Advance in Fracture Research", Vol. 4, Proceedings of the 7th ICF, 1989, edited by K. Salama *et al.* (Pergamon Press, 1989) p. 2927.
4. H. OHARA, A. T. YOKOBORI Jr, T. ADACHI, Y. AIZAWA and M. CHIKUNI, Preprint of the Annual Meeting of Japan Society for Strength of Materials (1987) p. 35.
5. T. YOKOBORI, *J. Phys. Soc. Jpn* **8** (1953) 104.
6. S. NAGASAKI (ed.), "Experiments of Metal Science" (Agne, 1964) (in Japanese).

Received 12 October
and accepted 19 November 1992